Journal of Electroceramics, 13, 463–469, 2004

Improved Electromechanical Response in Rhombohedral $BaTiO_3$

Y. AVRAHAMI & H.L. TULLER

Crystal Physics and Electroceramics Laboratory, Department of Materials Science and Engineering, MIT, Cambridge, MA 02139, USA

Submitted February 6, 2004; Revised November 20, 2003; Accepted December 16, 2003

Abstract. Zr-, Hf-, and KNb-doped $BaTiO_3$ materials were prepared in a composition range that stabilizes the rhombohedral phase above room temperature. These materials were prepared as bulk polycrystalline material using standard solid-state reaction methods. X-ray diffraction was used to confirm the existence of a stable rhombohedral phase while dielectric constant measurements confirmed the expected phase transition temperatures. A piezoelectric coefficient of $d_{33} = 290$–470 pC/N was obtained for Zr- and Hf-doped $BaTiO_3$, compared with $d_{33} = 75$ pC/N for pure $BaTiO_3$. An electrostrictive coefficient of $Q_{33} = 0.37$ m^4/C^2 was obtained for the KNb-doped material, compared with $Q_{33} = 0.11$ m^4/C^2 for pure $BaTiO_3$. The maximum strain measured for the doped samples was 5–10 times higher than that of pure $BaTiO_3$.

Keywords: piezoelectric, barium-titanate, dielectric, high strain

1. Introduction

$BaTiO_3$ based materials are of potential interest in a range of applications, including memory devices, tunable microwave dielectrics, and non-linear optics [1, 2]. The use of $BaTiO_3$ for piezoelectric applications is, however, limited due to the relatively small piezoelectric coefficient of the room temperature-stable tetragonal phase. In order to improve the piezoelectric response, efforts have been directed towards stabilizing the low-temperature rhombohedral phase. Stabilization of the rhombohedral phase can be achieved through the addition of Zr, Hf, $KNbO_3$, and Sn (see for example [3, 4]). Previous work has been done on some of these compositions for their dielectric properties [5]. More recently, we have proposed the use of the rhombohedral phase for its enhanced piezoelectric properties [6]. Recent work by Rehrig et al. [7] indicates that single crystals of Zr doped $BaTiO_3$ maintain a piezoelectric coefficient of 480 pC/N even when highly porous, compared to 190 pC/N for the undoped material.

2. Experimental

2.1. Sample Preparation

Samples were prepared by the solid-state reaction of precursor materials. Barium carbonate and potassium carbonate were used as sources for the A-site and metal oxides for the B-site ions. The desired molar ratio of powders was measured, and then ball milled and sieved to ensure small particle size. Powders were then pressed into pellets at 34.5 MPa (5000 psi), reacted at $T = 700^\circ$C and sintered at $T = 1200^\circ$C. The pellets were then ground, mixed, and sieved to achieve maximum uniformity and avoid porosity related to the solid state reaction. The powders were then uniaxially pressed at 48.3 MPa (7000 psi), followed by isopressing at 275.8 MPa (40000 psi), and sintering at a higher temperature. The pellets were held at 650°C to ensure complete binder burn-out prior to sintering at a temperature of 1300–1450°C. In some cases, a third firing step, identical to the second, was used in order to improve homogeneity further. A list of sample

Table 1. Polycrystalline sample compositions and sintering conditions.

Composition	x [%mol]	Sintering conditions
$Ba(Ti_{1-x}Zr_x)O_3$	7–15	3–4 hrs, 1400°C
$Ba(Ti_{1-x}Hf_x)O_3$	8–15	3–4 hrs, 1400–1450°C
$(BaTi)_{1-x}(KNb)_xO_3$	3.8, 4, 6	3 hrs, 1300°C

compositions and the corresponding sintering conditions are given in Table 1.

2.2. X-ray

Powder X-ray Diffraction (XRD) was used for structure and phase analysis. During cooling from the paraelectric phase, the crystalline symmetry of $BaTiO_3$ decreases. The result is splitting of the once degenerate cubic diffraction peaks. For the tetragonal phase the $\{100\}$ peaks become $\{100\}$ and $\{001\}$ while for the rhombohedral phase the $\{111\}$ splits into $\{111\}$ and $\{11\bar{1}\}$.

2.3. Dielectric Measurements

Dielectric measurements were performed using a Solartron 1260 impedance analyzer. Measurements at frequencies below 10 kHz, were limited due to the high resistivity of the sample. The sample resistivity was estimated to be higher than 10^8 Ωcm. In order to lower the impedance and enable a precise measurement of the capacitance, a 10 MΩ resistor was connected in parallel to the sample. The measured spectra for a sample with 11%Hf is shown in Fig. 1. The impedance of the capacitive component is given by:

$$Z'' = -\frac{1}{\omega C} \tag{1}$$

For the $BaTiO_3$:11%Hf sample, the equivalent circuit gave a capacity of $C = 9.88 \pm 0.02$ pF, while the value measured at 10 kHz without the 10 MΩ resistor was $C = 9.90$ pF. It is therefore possible to use a single frequency measurement on the sample itself in order to find the dielectric constant with little error. Dielectric constant measurements were thus performed as a function of temperature at a fixed frequency of 10 kHz on a series of compositions utilizing an HP4192 impedance analyzer to identify the phase transitions.

2.4. Piezoelectric Measurements

Electromechanical measurements were performed using a laser interferometery method. The Doppler shift between the sample and reference is translated into velocity, which is in turn integrated to calculate translation. A detailed description of the system and its components can be found in [8].

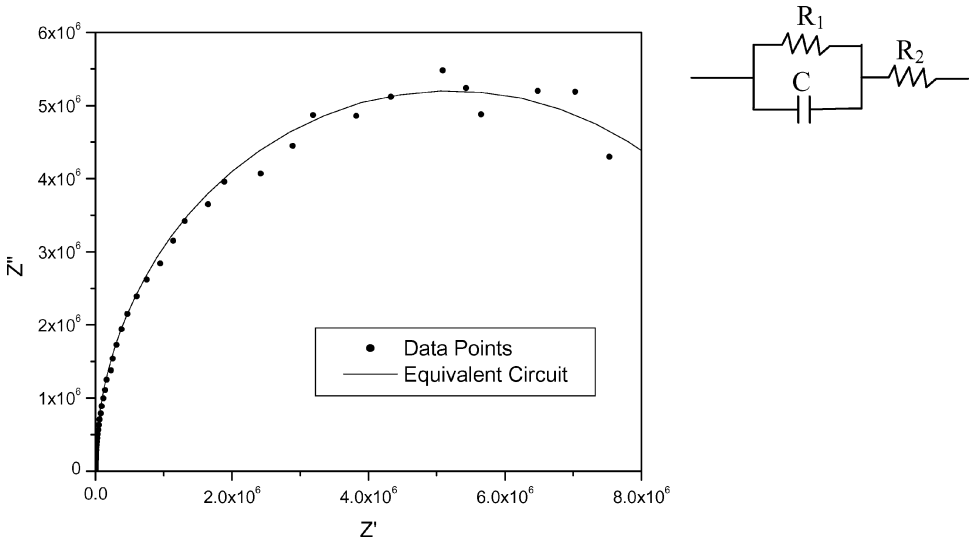

Fig. 1. Impedance plot for 11%Hf:$BaTiO_3$ with a 10 MΩ resistor in parallel. The equivalent circuit is $R_1 = 10 \pm .05$ MΩ, $R_2 = 1.5 \pm 0.1$ KΩ, and $C = 9.88 \pm 0.02$ pF.

A poling field of 10 kV/cm was chosen with the poling performed by cooling through the Curie temperature at 0.5°C/min under an applied electric field. A 1 kV/cm ac signal was added to the 10 kV/cm dc signal in order to improve the poling process [9].

The piezoelectric measurements were carried out in two modes: bi-polar (−V to +V) hysteresis loop and uni-polar (0 to +V) d_{33} measurement. The voltage amplitude was increased in steps of 0.5 kV until dielectric breakdown occurred. All the piezoelectric measurements were performed at 1 Hz and after the sample had sufficient time to cool from the poling process to below 25°C.

3. Results and Discussion

3.1. X-ray

X-ray diffraction spectra of "as-prepared" samples showed either tetragonal, rhombohedral or both phases. It is important to note that although different morphologies can co-exist, the samples did not reveal the presence of any minor phases.

Applying even a small poling field (as low as 1 kV/cm) reduced the stability of the tetragonal phase and X-ray spectra taken after poling show only the rhombohedral (111) split, as can be seen in Figs. 2 and 3.

The X-ray data was fitted to a rhombohedral unit cell with lattice parameter **a**, and angle α. The value of α was calculated first using the (111) and (222) lines [10]:

$$\cos\alpha_R = \frac{mN}{l\,(h+k) - m\cdot h\cdot k} \tag{2}$$

with:

$$m = \frac{\sin\theta_{hk\bar{l}} - \sin\theta_{hkl}}{\sin\theta_{hk\bar{l}} + \sin\theta_{hkl}} \qquad N = h^2 + k^2 + l^2 \tag{3}$$

Since m depends on the difference between θ_{hkl} and θ_{hk-l}, the resolution of the diffractometer determines the accuracy of measuring α. For some samples, especially at the higher doping level, no (111) or (222) peak splitting was observed and the pattern was similar to cubic. Since the dielectric measurements show that the material is already in the ferroelectric phase (see Section 3.2 below), this should be attributed to the resolution of the X-ray instrument, making it impossible to measure $\alpha \geq 89.99$.

Using the value of α, the lattice parameter was calculated according to:

$$a_R = \frac{\lambda\sqrt{N}}{2\sin\theta_{hkl}\left(1 + \frac{hk+kl+hl}{N}\cos\alpha_R\right)} \tag{4}$$

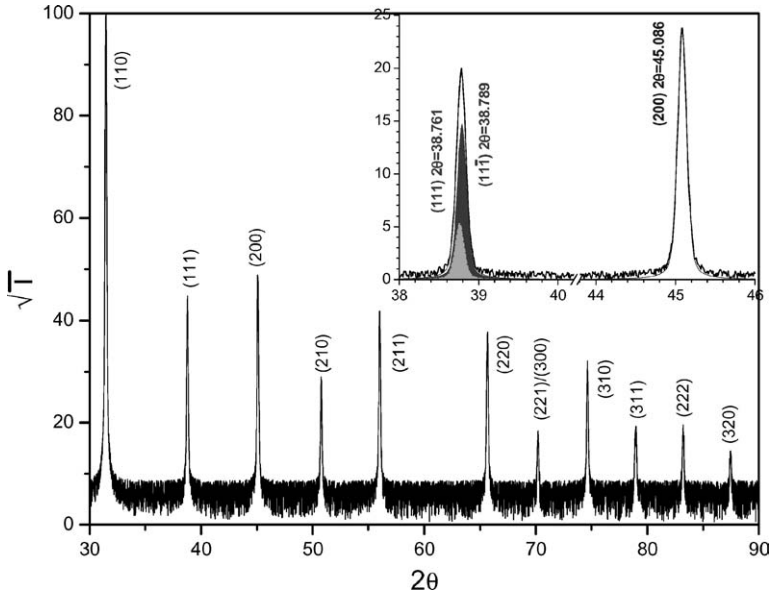

Fig. 2. X-ray diffraction spectrum for 8%Zr:$BaTiO_3$. The insert shows the fitting for the (111) and (200) peaks, matching a rhombohedral phase.

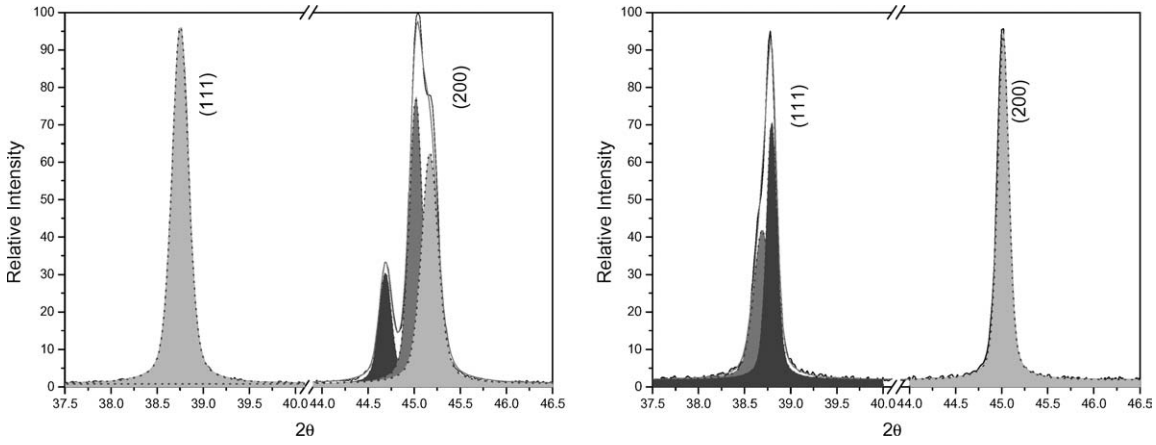

Fig. 3. X-ray diffraction spectrum of 10%Hf:$BaTiO_3$ showing both the tetragonal and rhombohedral splitting prior to poling (a), compared to only rhombohedral split after poling (b).

Table 2 summarizes the lattice parameter and rhombohedral angle measured in this work.

Using the molar fraction [Zr] and [Hf], the following linear fits were obtained for the rhombohedral lattice parameter:

$$a = 4.005 + (0.18 \pm 0.005) \cdot [Zr]\text{Å} \quad (5)$$

$$a = 4.008 + (0.17 \pm 0.005) \cdot [Hf]\text{Å} \quad (6)$$

In both cases the rhombohedral distortion was very small, with $89.95^\circ < \alpha < 90^\circ$. It is interesting to note that the volumetric lattice parameter ($\sqrt[3]{a^2c}$) for pure $BaTiO_3$ at room temperature is 4.006 Å–4.007 Å [11], compared to $(4.005 \pm 5 \times 10^{-4})$Å and $(4.008 \pm 5 \times 10^{-4})$Å in Eqs. (5) and (6).

3.2. *Dielectric Properties*

The temperature dependent dielectric constant measurements for Zr-doped $BaTiO_3$, as shown in Fig. 4, show a distinct Curie transition. Subsequent transitions, however, are less obvious. The derivative of the dielectric constant (ε') was taken in order to find these phase transitions. The transition temperatures extracted from these derivatives are compared to literature values in Fig. 5. The error in estimating the transition temperature from ε' is relatively small, $\pm 1^\circ$ for the Curie point and $\pm 2.5^\circ$ for the other transitions. This, however, is only part of the actual error. Having the thermocouple in contact with the sample introduced errors in the impedance measurement. The thermocouple was, therefore, not in direct contact with the sample, introducing an additional source of error. To maximize thermal equilibration, the heating rate was kept at 1–2°C/min. The overall error in temperature reading is estimated at no more ±3°C.

3.3. *Electromechanical Testing*

The polarization hysteresis loop was calculated by integrating the current during the piezoelectric testing. The hysteresis loop for Zr- and Hf-doped $BaTiO_3$ was very narrow, with a coercive field around 2–3 kV/cm. The samples doped with $KNbO_3$ showed an almost paraelectric response. The piezoelectric response was

Table 2. Summary of lattice parameter and rhombohedral angle for samples studied in this work.

	7% Zr	8% Zr	10% Zr	15% Zr	8% Hf	10% Hf	11% Hf	15% Hf	3.8% KN	4% KN
d [Å]	4.017	4.0185	4.023	4.031	4.0215	4.025	4.027	4.0335	4.009	4.006
α	89.95	89.97	≥89.99	≥89.99	89.965	89.98	89.985	≥89.99	≥89.99	≥89.99

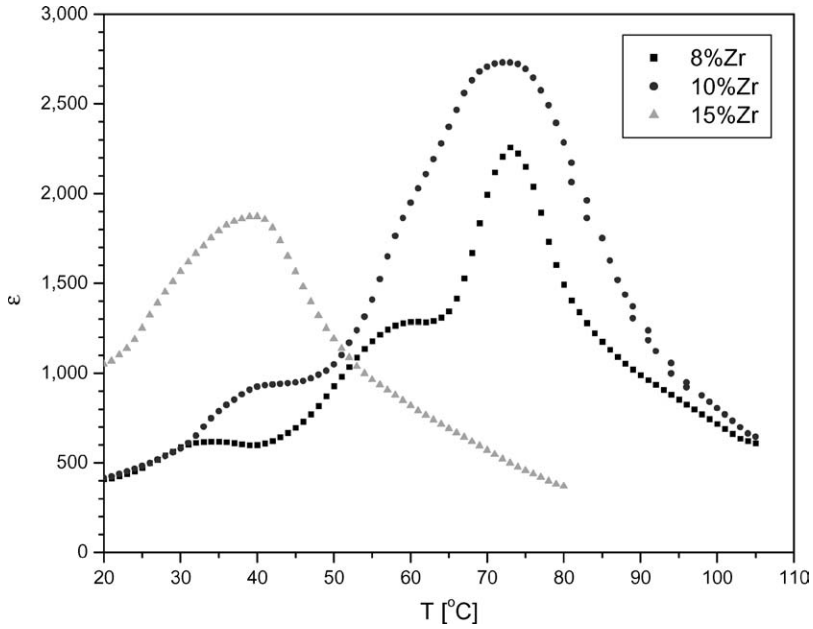

Fig. 4. Dielectric constant as a function of temperature for Zr doped $BaTiO_3$.

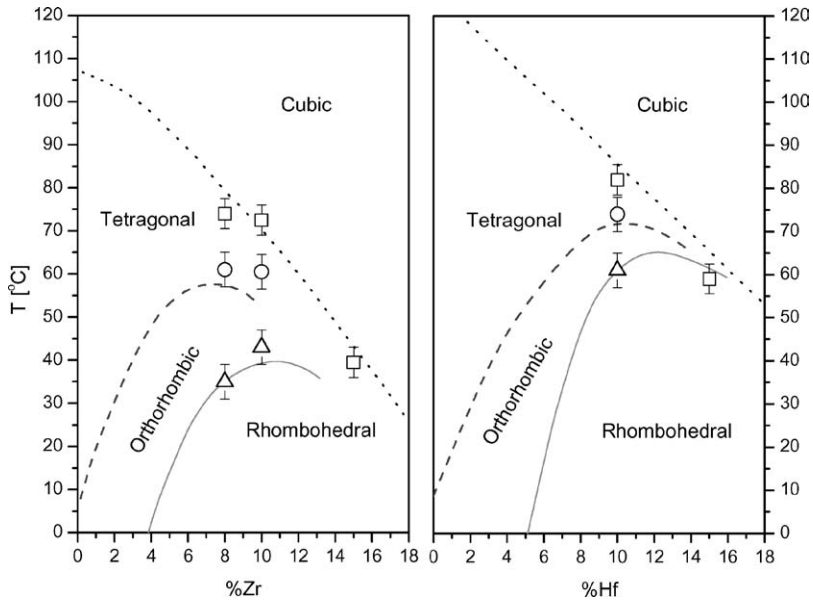

Fig. 5. Phase diagrams for $BaTiO_3$:$BaZrO_3$ (based on [3]) and $BaTiO_3$:$BaHfO_3$ (based on [4]) with results from the current work.

measured for the different samples and compared to that of standard PZT samples. A sample of pure $BaTiO_3$ was also prepared for comparison. Figure 6 shows the strain vs. field response for different materials. It can be seen that all the rhombohedral phase-stabilized $BaTiO_3$ samples show a significant enhancement in the strain achieved for a given applied field over that of the pure (tetragonal) phase.

All the doped samples showed a two stage piezoelectric response, with the boundary around 12 kV/cm. For Zr and Hf doping, the low field regime is dominated by a high piezoelectric response ($d_{33} > 300$ pC/N),

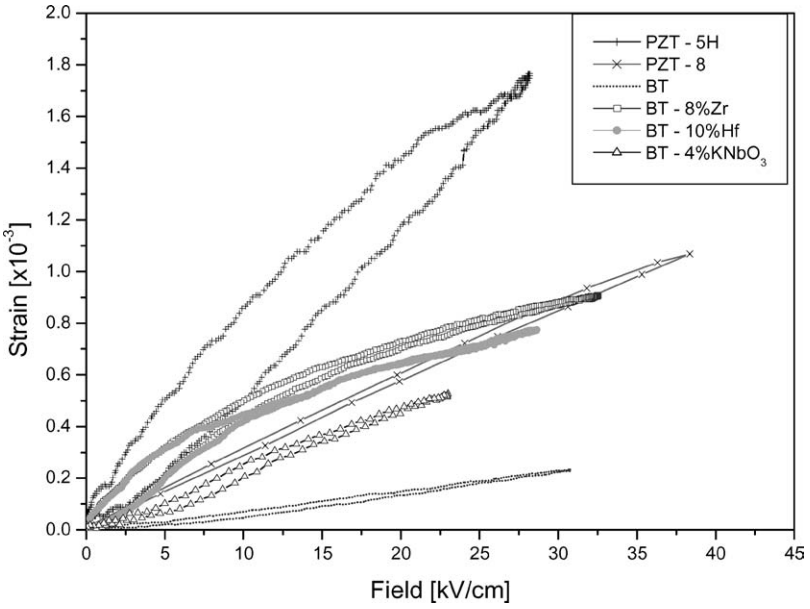

Fig. 6. Strain vs. electric field behavior of doped $BaTiO_3$ (4%$KNbO_3$, 8%Zr, 10%Hf) compared to standard PZT and pure $BaTiO_3$.

and the high field regime by a saturation level with $d_{33} < 100$ pC/N. The high field value is characteristic of pure $BaTiO_3$, suggesting that the material undergoes a phase transition into the tetragonal phase. As was mentioned earlier, the pinching of the phase stability regions can result in a meta-stable tetragonal phase at room temperature. This meta-stable phase suggests that the rhombohedral and tetragonal phases have similar free energy states, allowing for a field induced phase transition. A field induced phase transition is usually accompanied by a sharp increase in strain. Such a step is not observed in Fig. 6, but rather a more continuous increase. This suggests that sample inhomogeneity may be playing a significant role in the electro-mechanical response. For a sample with a range of compositions, each composition will have a different field required for inducing a transition, resulting in a smoothing effect on the strain vs. field behavior.

The low hysteresis observed in the dielectric measurements of $KNbO_3$ doped $BaTiO_3$ is also reflected in the piezoelectric measurement. For low field, the sample was fitted to a second order polynomial. The response is mostly electrostrictive, with $Q_{11} = (0.37 \pm 0.3)$ m^4/C^2 or $M_{11} = (1.7 \pm 0.3) \times 10^{-16}$ C^2/N^2, with a small piezoelectric contribution, $d_{33} = (7 \pm 0.5)$ pC/N. The electrostriction coefficient is 3.5 times higher than the value reported for pure $BaTiO_3$, $Q_{11} = 0.11$ m^4/C^2 [12]. From the relationship between M and Q, one can find the dielectric constant:

$$\varepsilon = \frac{1}{\varepsilon_0}\sqrt{\frac{M}{Q}} = 2400 \tag{7}$$

The reason for the electrostrictive behavior is not clear. Although the X-ray diffraction is indistinguishable from the cubic phase, a Curie transition is seen in the dielectric measurements. A tetragonal distortion, even a small one, will be visible in the diffraction data. It is therefore reasonable to assume that the sample is indeed rhombohedral. The small distortion, however, might not be enough to create a strong piezoelectric response. Another option is that the dual ion replacement is responsible for the electrostriction. Both theories require more research for verification.

At the higher field regime the 4%KN:$BaTiO_3$ becomes piezoelectric, with $d_{33} = 215$ pC/N. The transition field is similar to that observed in Zr and Hf doped materials, suggesting that this is also due to a phase transition. This specimen underwent dielectric breakdown at a lower field then the other compositions, making it unclear if the high field piezoelectric constant reaches saturation as for the other compositions.

Table 3. Summary of the piezoelectric constant (d_{33}) and maximum strain (X_{max}) for the different compositions studied. In some cases a low field and high field value is given if the slope changed significantly.

	BT 7%Zr	BT 8%Zr	BT 10%Hf	BT 11%Hf	BT 4%KN	Pure BT	PZT 5H	PZT 8
d_{33} [pC/N]	450/75	470/90	450/80	460/85	7*/215	75 (190**)	600	250
X_{max}	9×10^{-4}	1×10^{-3}	1.1×10^{-3}	8×10^{-4}	6×10^{-4}	1.5×10^{-4}	1.8×10^{-3}	1.1×10^{-3}

* This is the linear component in low field electrostrictive fitting.
** Sample measured as 75 pC/N, literature value is 190 pC/N [11].

Table 3 summarizes the piezoelectric response for the different samples examined. It can be seen that the rhombohedral phase outperforms pure $BaTiO_3$, both in respect to d_{33} and maximum strain, by almost an order of magnitude. This suggests that these $BaTiO_3$-based materials may compete with hard PZT (PZT8) particularly where Pb-free materials are preferred.

4. Conclusions

$BaTiO_3$ was modified to stabilize the rhombehedral phase above room temperature by the addition of Zr-, Hf-, and KNb. Temperature dependent dielectric measurements in conjunction with X-ray diffraction confirmed the achievement of the desired rhombohedral phase together with the expected transition temperatures. The rhombohedral phase was found to exhibit surperior electromechanical properties. A piezoelectric coefficient of $d_{33} = 290$–470 pC/N was obtained for Zr- and Hf-doped $BaTiO_3$, compared with $d_{33} = 75$ pC/N for pure $BaTiO_3$. An electrostrictive coefficient of $Q_{33} = 0.37$ m^4/C^2 was obtained for the KNb-doped material, compared with $Q_{33} = 0.11$ m^4/C^2 for pure $BaTiO_3$. The maximum strain measured for the doped samples was 5–10 times higher than that of pure $BaTiO_3$.

Acknowledgment

This work was supported by the Army Research Office under grant # DAAH04-95-1-0104).

References

1. H.S. Nalwa (ed.), *Ferroelectric and Dielectric Thin Films*, vol. 3, in *Handbook of Thin Film Materials* (Academic Press, London, 2002).
2. P.C. Joshi and M.W. Cole, *Applied Physics Letters*, **77**, 289 (2000).
3. T.N. Verbitskaia, G.S. Zhdanov, I.N. Venevtsev, and S.P. Soloviev, *Soviet Phys. Cryst.*, **3**, 182 (1958).
4. W.H. Payne and V.J. Tennery, *Journal of the American Ceramic Society*, **48**, 413 (1965).
5. V. Tura, L. Mitoseriu, C. Harnagea, and D. Ricinschi, *Ferroelectrics*, **239**, 265 (2000).
6. Y. Avrahami and H. Tuller, pat. no. 6,526,833 (2003).
7. P.W. Rehrig, S.-E. Park, S. Trolier-McKinstry, G.L. Messing, B. Jones, and T.R. Shrout, *Journal of Applied Physics*, **86**, 1657 (1999).
8. B.P. Nunes (Massachusetts Institute of Technology, Cambridge, 2001).
9. M. Sayer, B.A. Judd, K. El-Assal, and E. Prasad, *Journal of the Canadian Ceramic Society*, **50**, 23 (1981).
10. B.D. Cullity, *Elements of x-ray Diffraction* (Addison-Wesley Pub. Co., Reading, Mass., 1978).
11. B. Jaffe, W.R. Cook, and H. Jaffe, *Piezoelectric Ceramics* (Academic Press, New York, 1971).
12. K. Uchino, *Piezoelectric Actuators and Ultrasonic Motors* (Kluwer Academic Publisher, Boston, 1997).